

Dynamical Insights into Oxygen Diffusion in BaTiO3 and SrTiO₃

James Alexander Dawson

Oxygen diffusion is a key process in BaTiO₃ and SrTiO₃ that determines many of their important electronic properties. Despite the importance of oxygen diffusion in these systems, there is still currently significant variation in the oxygen diffusion coefficients for BaTiO₃ and SrTiO₃ reported in the literature from both experimental and computational methods. Using molecular dynamics simulations, the effect of oxygen vacancy concentration on the oxygen diffusion properties is investigated for these perovskite materials. Oxygen diffusion coefficients and activation energies for both materials are calculated over a temperature range of 900-1500 K. Oxygen vacancy charge compensation is achieved by the reduction of Ti⁴⁺ to Ti³⁺ ions, in agreement with experimental results for undoped BaTiO₃ and SrTiO₃. The findings from this study yield an accurate reference point for the calculation of oxygen diffusion in these materials and also the application of molecular dynamics in studying such phenomena.

1. Introduction

Many of the fundamental properties and applications of perovskite materials are a result of diffusion. An understanding of oxygen diffusion in materials such as BaTiO3 and SrTiO3 is therefore important for their electrochemical applications. Oxygen diffusion is especially important in the main commercial use of BaTiO₃ in multilayer ceramic capacitors (MLCCs). BaTiO₃-based compositions are often cofired with Ni electrodes in a reducing atmosphere to avoid oxidation of Ni. [1,2] This reducing environment causes the formation of oxygen vacancies that must be charge compensated by electrons. In this material, they are assumed to be small polarons and are represented by the reduction of Ti⁴⁺ to Ti³⁺ ions. However, these vacancies can seriously reduce the performance of the capacitor over its lifetime^[3-5] and so acceptor dopants (e.g., rare Earth [RE]) are introduced to reduce the concentration of these oxygen vacancies. These dopants have been shown to significantly reduce the oxygen diffusivity^[6,7] and therefore increase the service time of these devices. Establishing the mechanisms and rates of oxygen diffusion in BaTiO3 is essential to improve our understanding of degradation phenomena in these ubiquitous devices.

Dr. J. A. Dawson Department of Chemistry University of Bath Bath, BA2 7AY, UK E-mail: j.a.dawson@bath.ac.uk

The ORCID identification number(s) for the author(s) of this article can be found under https://doi.org/10.1002/pssb.201900422.

DOI: 10.1002/pssb.201900422

SrTiO₃ also has a variety of interesting electrical properties, including straininduced ferroelectricity for microwave devices^[8] and a high relative permittivity for use in random access memory.[9] Reduced SrTiO₃ has a high Seebeck coefficient, necessary for thermoelectric applications. [10] SrTiO₃ was also the first ternary oxide discovered to be superconducting.[11] Like BaTiO₃, many of the interesting features of SrTiO₃ are a result of its transport properties and in particular the transport properties of the most abundant defects in SrTiO₃, oxygen vacancies.^[12,13] For example, doped SrTiO₃ can be used as a varistor when prepared in a reducing atmosphere. In this application, the creation of oxygen vacancies is accompanied by a compensating electronic polaron, but instead of hin-

dering the device as in the case of BaTiO3-based MLCCs, these vacancies help to create the required semiconducting grains. [14] SrTiO₃ also receives attention because of its ability to act as a reference system for mixed conductors and other related perovskite systems. [15,16] Recently, SrTiO₃ has received additional interest because of its potential application in all-oxide electronics and as a memresistive element. [15,17,18] For both of these uses, an understanding of oxygen diffusion is paramount.

There are large variations in the experimentally measured chemical and self/tracer diffusion for both doped and undoped BaTiO₃ and SrTiO₃. A compilation of diffusion data for BaTiO₃ from the literature is given in ref. [1]. For the tracer diffusion of oxygen, three data sets are provided, with the values quoted varying in magnitude significantly. For example, the diffusion data of Shirasaki et al.^[7] show an increase in diffusivity with temperature over a range of 1100-1700 K, with the oxygen diffusion coefficient ($D_{\rm O}$) ranging from $\approx 5 \times 10^{-13}$ to $1 \times 10^{-12} \,\mathrm{cm^2 \, s^{-1}}$. However, later results from Shirasaki et al. [19] show a far greater range of $D_{\rm O}$ over \approx 1000–1700 K $(\approx 10^{-14} - 10^{-10} \text{ cm}^2 \text{ s}^{-1})$. The tracer diffusion coefficient of oxygen has also been reported to be $\approx 2 \times 10^{-11} \, \text{cm}^2 \, \text{s}^{-1}$ elsewhere. [20,21] The oxygen self-diffusion activation energy has been found to be 0.5 eV in both single-crystal and polycrystalline samples.[22]

A similar level of variation in the oxygen diffusion coefficients for $SrTiO_3$ also exists, as shown by the collection of experimental data presented by Pasierb et al. [23] Generally, the results show higher values for DO compared with the values for BaTiO₃. Similar to BaTiO₃, the increase in diffusivity with temperature is far greater in some cases. For example, ref. [23] shows values of DO that increase by approximately three orders of

stat soli

www.pss-b.com

magnitude (10^{-11} – 10^{-8} cm² s⁻¹) over a temperature range of ≈ 300 K, whereas over a larger temperature range (≈ 600 K), other $D_{\rm O}$ data show an increase of less than two orders of magnitude (10^{-11} – 10^{-9} cm² s⁻¹). A more recent study reports the oxygen tracer diffusion coefficient in single-crystal SrTiO₃ to be $\approx 1 \times 10^{-11}$ cm² s⁻¹ with only a small increase with increasing temperature (950–1150 K). An oxygen vacancy migration energy of 0.6 eV was calculated from this data.

While there are numerous computational investigations of oxygen diffusion in these perovskites,^[12,24–31] studies with excellent agreement with experimental results are limited. Kubo et al.^[27] performed molecular dynamics (MD) calculations on barium and oxygen diffusion in BaTiO₃, as well as for strontium and oxygen diffusion in SrTiO₃; however, no diffusion activation energies were calculated. Calculations by Lewis et al.^[28] estimated that the activation energy of oxygen vacancy diffusion in BaTiO₃ is 0.62 eV. An activation energy of 0.93 eV for oxygen vacancy migration was derived for SrTiO₃ from MD calculations.^[29] Akhtar et al.^[12] used lattice statics to calculate an oxygen vacancy activation energy of 0.75 eV for SrTiO₃. Density functional theory (DFT) calculations of SrTiO₃ have estimated the oxygen migration energy to be between 0.4 and 0.7 eV.^[30,31]

In this work, MD simulations are used to calculate diffusion coefficients and activation energies for a range of oxygen vacancy concentrations. The calculations present good agreement with experimental results, particularly for the lowest oxygen vacancy concentration of 2%. The results from this work help to provide a better understanding of oxygen diffusion in these materials.

2. Methodology

To accurately model these perovskite materials, a potential model developed to study RE doping of cubic BaTiO₃ and SrTiO₃ is used. [32–37] This potential has also been extended to study a variety of other defect and doping phenomena, including transition metal doping of BaTiO₃ and SrTiO₃ [38,39] and the effects of RE ion size [40] and A-site mixing [41] on the Curie temperature of BaTiO₃. Unlike earlier BaTiO₃ and SrTiO₃ potential models, this model uses a Lennard–Jones potential to model the Ti–O interaction. This type of potential was chosen as, unlike a Buckingham potential, a Lennard–Jones potential generates a potential energy well that represents the bonding character shown to be present in the Ti–O interaction by DFT simulations. [42] A three-body term O–Ti–O was also used to provide further rigidity to the TiO₆ octahedra and was fitted using Hartree–Fock unrestricted single-point calculations.

A Buckingham potential was used to model both the Ba–O and Sr–O interactions as no covalency has been observed for these interactions. The O–O Buckingham potential was taken from Lewis and Catlow^[43] to ensure consistency between other oxide materials and defect-oxygen interactions. The Ti–O, Ba–O, and Sr–O potential parameters were fitted to give accurate values for the cohesive energies and lattice parameters of BaTiO₃, SrTiO₃, and the associated end members, TiO₂ (rutile), BaO, and SrO.^[32,34] A Monte Carlo algorithm was used to vary both the Buckingham and Lennard–Jones potential parameters to ensure the best fit to experimental data.^[32] A cutoff distance of 12 Å is used for all the potentials.

The calculations here were completed using the widely available MD code, DL_POLY_2.[44] The ions are treated as rigid spheres in these calculations (i.e., the rigid ion model $[^{45}]$). Supercells of $7 \times 7 \times 7$ (1715 atoms) were used for the calculations. A random distribution of oxygen vacancies was inserted into each starting configuration at a concentration of 2%, 3%, or 5%. These vacancies were charge compensated by the reduction of selected Ti⁴⁺ to Ti³⁺ ions, as confirmed experimentally. The Ti³⁺ ions were distributed randomly at Ti sites throughout the supercells and their interaction with oxygen was modeled explicitly with a Ti³⁺-O²⁻ Buckingham potential from Lewis and Catlow. [43] A random distribution of reduced Ti ions was chosen to avoid significant binding between localized defects that may result in oxygen trapping. Furthermore, the use of localized Ti³⁺ sites would not necessarily be valid given that the oxygen exhibits long-range transport.

The starting configurations for all the MD simulations were optimized using the General Lattice Utility Program (GULP)^[46] to start the simulation in the minimum energy state for that particular configuration. An equilibration time of 20 ps was used for each simulation with a total run time of 2 ns. A time step of 1 fs was used for all the calculations. The canonical NPT ensemble and the Nose–Hoover thermostat/barostat with a relaxation time of 0.1 ps for both the thermostat and barostat are used in all calculations. The self-diffusion data for oxygen were obtained from a mean square displacement (MSD) analysis according to

$$r_i^2(t) = 6D_0 t \tag{1}$$

where $r_{\rm i}^2(t)$ is the MSD, $D_{\rm O}$ is the diffusion coefficient for oxygen, and t is time. The MSDs were produced by measuring and combining the displacements of individual oxygen ions. Similar approaches have been utilized to study ion diffusion in a wide variety of materials.^[47–54]

3. Results and Discussion

3.1. Thermal Expansion of BaTiO₃ and SrTiO₃

The coefficient of thermal expansion provides a good measure of whether a potential set is capable of accurately reproducing basic macroscopic properties. The calculated thermal expansion coefficients of cubic $BaTiO_3$ and $SrTiO_3$ from 300 to 1500 K are given in **Figure 1**.

For BaTiO₃, a volume thermal expansion coefficient of $1.63 \times 10^{-5}~\text{K}^{-1}$ and a linear thermal expansion coefficient of $0.54 \times 10^{-5}~\text{K}^{-1}$ are calculated. There is a large range of experimental values for the linear thermal expansion coefficient that vary significantly with temperature, grain size, and structure. Xiao et al. [55] recorded values ranging from $0.23 \times 10^{-5}~\text{K}^{-1}$ for samples with large grain sizes at a sintering temperature of 1200~°C to $0.73 \times 10^{-5}~\text{K}^{-1}$ for samples with smaller grains at a sintering temperature of 1000~°C. In another study of the thermal properties of BaTiO₃, a linear thermal expansion coefficient of $\approx 0.6 \times 10^{-5}~\text{K}^{-1}$ was observed at room temperature where BaTiO₃ is ferroelectric. [56] However, beyond the ferroelectric Curie temperature (i.e., the cubic structure), the value for linear expansion rises to $\approx 1.1 \times 10^{-5}~\text{K}^{-1}$. Kubo et al. [27] used

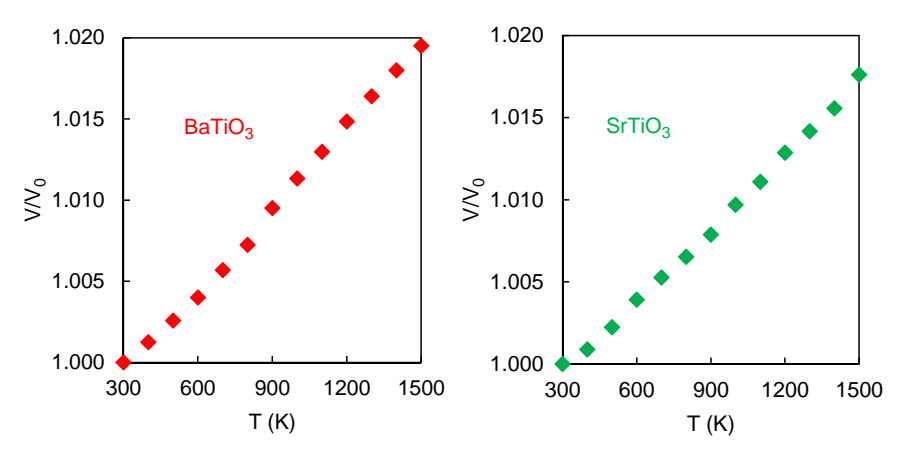


Figure 1. Volume thermal expansion as a function of temperature for cubic BaTiO₃ and SrTiO₃.

MD calculations to calculate a linear thermal expansion coefficient of $1.22\times10^{-5}\,\text{K}^{-1}.$

For SrTiO₃, a volume expansion coefficient of $1.47 \times 10^{-5} \, \text{K}^{-1}$ and a linear expansion coefficient of $0.49 \times 10^{-5} \, \text{K}^{-1}$ are found. These values are slightly smaller than those obtained for BaTiO₃, which suggests that expansion of the smaller, more coulombically bound SrTiO3 is somewhat inhibited in comparison with BaTiO₃. This is supported by experimental results where volume thermal expansion coefficients of $2.16-3.23 \times 10^{-5} \, \text{K}^{-1}$ (with equivalent linear values of $0.72-1.08 \times 10^{-5} \, \mathrm{K}^{-1}$) were obtained. [57] Some deviation from experimental results is to be expected for the calculated values given that polycrystalline SrTiO₃ samples will contain defects, dopants, and microstructural features, such as grain boundaries, whereas the simulated system is pristine. Previous MD calculations $^{[58]}$ produced a linear expansion coefficient of $0.57 \times 10^{-5} \,\mathrm{K}^{-1}$ for SrTiO₃, which is in excellent agreement with the value in this work. The agreement between the values in this work and literature values suggests that the potential set is capable of reproducing the basic structural properties of these materials.

3.2. Oxygen Diffusion in BaTiO₃

The diffusion of oxygen in cubic BaTiO₃ cells with 2%, 3%, and 5% oxygen ions removed was studied. These values were chosen to give a wide range of data so that the influence of the oxygen vacancy ($V_{\rm O}$) concentration can be assessed. Experimentally, BaTiO₃ samples with oxygen deficiency levels of up to $\approx 5.7\%$ can be formed. ^[59] Charge compensation in such samples comes from electronic compensation (the partial reduction from Ti⁴⁺ to Ti³⁺), ^[60] which is modeled explicitly using a Ti³⁺–O²⁻ potential taken from Lewis and Catlow. ^[43]

An example MSD plot for an oxygen vacancy concentration of 2% is given in Figure 2. The final 10% of the simulation time has been removed because of the poor statistics usually associated with the final section of an MSD calculation. All the MSD plots increase linearly with time and therefore oxygen ions exhibit migration through the system. Unsurprisingly, the diffusivity increases in systems with higher concentrations of $V_{\rm O}$. To appreciate the true effects of the oxygen vacancy concentration, the diffusion coefficients and activation energies must be calculated.

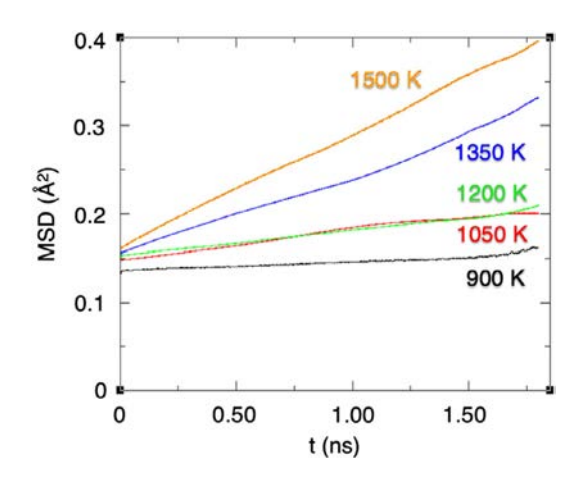


Figure 2. MSD of oxygen in $BaTiO_3$ with a 2% V_O concentration.

The diffusion coefficients for oxygen were calculated using Equation (1) for each of the $V_{\rm O}$ concentrations and are given in **Table 1**. Reducing the $V_{\rm O}$ concentration also reduces the oxygen diffusivity because of the smaller concentration of defects that are available for migration. This illustrates the importance of choosing a wide range of $V_{\rm O}$ concentrations in these calculations and also how the calculated diffusion coefficients can be used to find the $V_{\rm O}$ concentration that best fits to experimental data.

Table 1. Oxygen diffusion coefficients (D_O) for BaTiO₃.

Temperature [K]	$D_{\rm O}$ [cm ² s ⁻¹]		
	5% V _O	3% V _O	2% V _O
900	$4.33 \pm 1.39 \times 10^{-10}$	$3.01 \pm 1.21 \times 10^{-10}$	$1.52 \pm 0.30 \times 10^{-10}$
1050	$6.67 \pm 1.27 \times 10^{-10}$	$5.67 \pm 1.53 \times 10^{-10}$	$5.48 \pm 1.37 \times 10^{-10}$
1200	$1.23 \pm 0.16 \times 10^{-9}$	$8.33 \pm 1.33 \times 10^{-10}$	$5.16 \pm 0.74 \times 10^{-10}$
1350	$1.73 \pm 0.23 \times 10^{-9}$	$1.43 \pm 0.14 \times 10^{-9}$	$2.06 \pm 0.25 \times 10^{-9}$
1500	$3.17 \pm 0.38 \times 10^{-9}$	$2.33 \pm 0.19 \times 10^{-9}$	$2.32 \pm 0.23 \times 10^{-9}$

Solidi States Promised Parisical Physical Physic

By comparing the simulation results to experimental measurements of oxygen tracer diffusion, $^{[1]}$ as discussed in the introduction, it can be seen that the lowest $V_{\rm O}$ concentration of 2% presents the best agreement. For the 900–1200 K temperature range, the calculated diffusion coefficients are around an order of magnitude greater than the experimental results presented in ref. [1]. At higher temperatures, the agreement is excellent.

The oxygen diffusion activation energies ($E_{\rm act}$) calculated for $V_{\rm O}$ concentrations of 2%, 3%, and 5% are 0.53, 0.39, and 0.38 eV, with the Arrhenius plots shown in **Figure 3**. The activation energies increase with reducing $V_{\rm O}$ concentration, as expected. The largest activation energy of 0.53 eV is found for the 2% $V_{\rm O}$ concentration.

As discussed, there is a large range of calculated experimental and theoretical activation energies in the literature for oxygen diffusion. Lin et al. [61] provides an overview of some of the previously reported values that have been obtained using various different methods. These values range from 0.44 eV [7] (tracer diffusion experiments) to 4.86 eV [62] (sintering model). The calculated value of 0.53 eV is in excellent agreement with the tracer diffusion value. When considering activation energies, self-diffusion data are often considered comparable with tracer diffusion because the activation energies are not usually affected by correlation effects and therefore it is reasonable to compare values from the two methods. Other activation energies obtained from self-diffusion measurements (0.55 eV) [21] and lattice statics calculations (0.62 eV) [63] are also in good agreement.

3.3. Oxygen Diffusion in SrTiO₃

For SrTiO₃, grossly nonstoichiometric samples with up to \approx 9.5% oxygen deficiency can be formed.^[64] It is clear that Ti³⁺ charge compensation is correct for BaTiO₃, and it is well known experimentally.^[65,66] that this is also the correct mechanism for SrTiO₃. The MSD for oxygen in cubic SrTiO₃ with 2% $V_{\rm O}$ is shown in **Figure 4**.

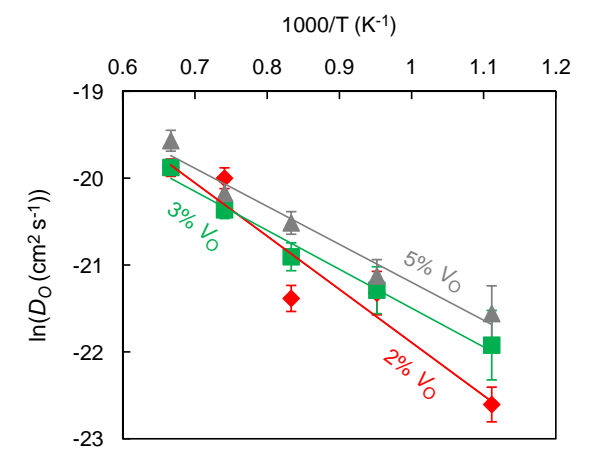


Figure 3. Arrhenius plots of $\ln(D_0)$ against 1/T for BaTiO₃ as a function of oxygen vacancy concentration.

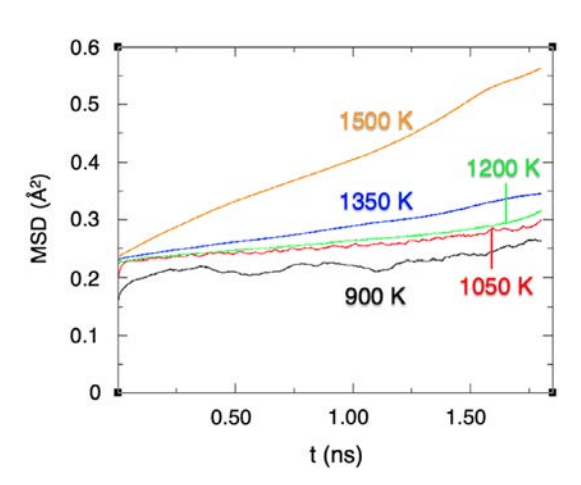


Figure 4. MSD of oxygen in $SrTiO_3$ with a 2% V_O concentration.

The oxygen diffusion coefficients for SrTiO₃ are shown in **Table 2**. Generally, there is a decrease in the diffusion rate with decreasing $V_{\rm O}$ concentration, as also observed for BaTiO₃. Comparison of $D_{\rm O}$ values in SrTiO₃ and BaTiO₃ shows that oxygen diffusion is overall higher in SrTiO₃. De Souza et al. [15] measured the bulk tracer diffusion coefficient of oxygen for temperatures between 950 and 1150 K. Their values ranged between 1 and $3 \times 10^{-11} \, {\rm cm}^2 \, {\rm s}^{-1}$. Similar to BaTiO₃, the calculated values are within an order of magnitude of these experimental results. Other experimental results show very good agreement with the calculated results, especially for 1200–1500 K. [23] The agreement between the computational and experimental data for the diffusion coefficients is generally better for SrTiO₃ than for BaTiO₃.

The oxygen diffusion activation energies (E_{act}) calculated for SrTiO₃ are 0.50, 0.46, and 0.30 eV for V_O concentrations of 2%, 3%, and 5%, respectively, with the Arrhenius plots shown in **Figure 5**. Similar to BaTiO₃, a reduction in the V_O concentration causes a significant increase in E_{act} .

De Souza et al. [15] obtained a value of 0.58 eV for the activation enthalpy of oxygen isotopes. From this value, a value of \approx 0.6 eV was calculated for the $V_{\rm O}$ migration energy. The work of De Souza et al. also presents a compilation of $V_{\rm O}$ migration energies, these values range from 0.3 to 2.1 eV for experimental methods and from 0.4 to 1.35 eV for DFT and pair-potential calculations. The calculated value of 0.5 eV is in excellent agreement with these values.

Table 2. Oxygen diffusion coefficients (D_O) for SrTiO₃.

D_{O} (cm ² s ⁻¹)				
Temperature [K]	5% V _O	3% V _O	2% V _O	
900	$6.67 \pm 2.40 \times 10^{-10}$	$3.33 \pm 0.87 \times 10^{-10}$	$1.60 \pm 0.66 \times 10^{-10}$	
1050	$1.27 \pm 0.24 \times 10^{-9}$	$5.67 \pm 1.30 \times 10^{-10}$	$4.53 \pm 1.18 \times 10^{-10}$	
1200	$1.57 \pm 0.31 \times 10^{-9}$	$1.13 \pm 0.22 \times 10^{-9}$	$5.50\pm1.10\times10^{-10}$	
1350	$1.87 \pm 0.34 \times 10^{-9}$	$2.13 \pm 0.36 \times 10^{-9}$	$9.62 \pm 1.73 \times 10^{-10}$	
1500	$3.90 \pm 0.59 \times 10^{-9}$	$3.33 \pm 0.40 \times 10^{-9}$	$2.99 \pm 0.75 \times 10^{-9}$	

15213951, 2020, 1, Downloaded from https:

://onlinelibrary.wiley.com/doi/10.1002/pssb.201900422 by Egyptian National Sti. Network (Enstinet), Wiley Online Library on [12/03/2023]. See the Terms and Conditions (https://onlinelibrary.wiley.com/doi/10.1002/pssb.201900422 by Egyptian National Sti. Network (Enstinet), Wiley Online Library on [12/03/2023]. See the Terms and Conditions (https://onlinelibrary.wiley.com/doi/10.1002/pssb.201900422 by Egyptian National Sti. Network (Enstinet), Wiley Online Library on [12/03/2023]. See the Terms and Conditions (https://onlinelibrary.wiley.com/doi/10.1002/pssb.201900422 by Egyptian National Sti. Network (Enstinet), Wiley Online Library on [12/03/2023]. See the Terms and Conditions (https://onlinelibrary.wiley.com/doi/10.1002/pssb.201900422 by Egyptian National Sti. Network (Enstinet), Wiley Online Library on [12/03/2023]. See the Terms and Conditions (https://onlinelibrary.wiley.com/doi/10.1002/pssb.201900422 by Egyptian National Sti. Network (Enstinet), Wiley Online Library on [12/03/2023]. See the Terms and Conditions (https://onlinelibrary.wiley.com/doi/10.1002/pssb.20190042).

onditions) on Wiley Online Library for rules of use; OA articles are governed by the applicable Creative Commons

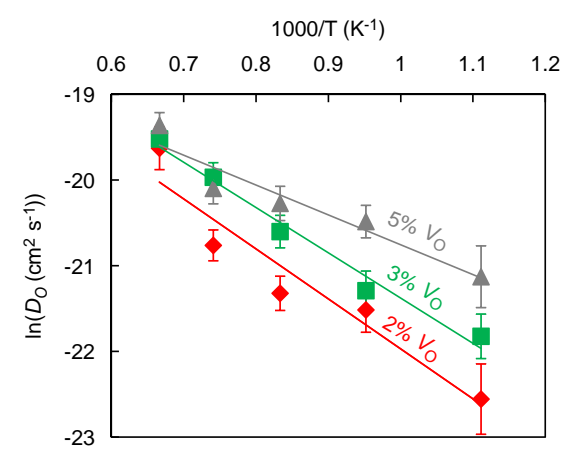


Figure 5. Arrhenius plots of $ln(D_O)$ against 1/T for $SrTiO_3$ as a function of oxygen vacancy concentration.

4. Conclusions

In this study, MD simulations have been used to study oxygen diffusion in BaTiO₃ and SrTiO₃. Oxygen vacancy concentrations ranging from 2% to 5% were simulated to best assess its effect on oxygen diffusion. Oxygen diffusion coefficients were calculated from MSD plots for each oxygen vacancy concentration over a temperature range of 900–1500 K. Arrhenius plots of the diffusion coefficients were then used to calculate the activation energy of oxygen diffusion for these materials.

The calculations for BaTiO₃ and SrTiO₃ confirmed the experimentally proven compensation mechanism of Ti⁴⁺ reduction to Ti³⁺ ions, producing excellent agreement for the activation energies compared with experimental values. The lowest oxygen vacancy concentration tested (2%) gave both the closest diffusion and activation energy data to experimental results. The activation energy for oxygen diffusion in these materials increased with decreasing oxygen vacancy concentration. It was found that for both perovskites, the diffusion coefficients at lower temperatures (900–1050 K) are about an order of magnitude higher than experimental values. Although at higher temperatures (1200–1500 K), the agreement is much better, especially for SrTiO3. The agreement for the activation energies with experimental results and other simulations is excellent. These findings provide an important benchmark for both future modeling and experimental measurements of oxygen diffusion in solid-state materials and clearly illustrate the importance in considering a range of vacancy concentrations when investigating ion transport in such materials.

Acknowledgements

The author thanks the Engineering and Physical Sciences Research Council for funding from EPSRC grant EP/G005001/1.

Conflict of Interest

The author declares no conflict of interest.

Keywords

ion transport, multilayer ceramic capacitors, molecular dynamics, perovskites

Received: July 12, 2019 Revised: October 7, 2019 Published online: October 17, 2019

- [1] H.-I. Yoo, D.-K. Lee, Phys. Chem. Chem. Phys. 2003, 5, 2212.
- [2] T. Oyama, N. Wada, H. Takagi, Phys. Rev. B 2010, 82, 134107.
- [3] T. Baiatu, R. Waser, K.-H. Härdtl, J. Am. Ceram. Soc. 1990, 73, 1663.
- [4] R. Waser, T. Baiatu, K.-H. Härdtl, J. Am. Ceram. Soc. 1990, 73, 1645.
- [5] M. Kessel, R. A. De Souza, M. Martin, Phys. Chem. Chem. Phys. 2015, 17, 12587.
- [6] Y. Sakabe, Y. Hamaji, H. Sano, N. Wada, Jpn. J. Appl. Phys. 2002, 41, 5668
- [7] S. Shirasaki, H. Yamamura, H. Haneda, K. Kakegawa, J. Moori, J. Chem. Phys. 1980, 73, 4640.
- [8] J. H. Haeni, P. Irvin, W. Chang, R. Uecker, P. Reiche, Y. L. Li, S. Choudhury, W. Tian, M. E. Hawley, B. Craigo, A. K. Tagantsev, X. Q. Pan, S. K. Streiffer, L. Q. Chen, S. W. Kirchoefer, J. Levy, D. G. Schlom, *Nature* 2004, 430, 758.
- [9] A. A. Sirenko, C. Bernhard, A. Golnik, A. M. Clark, J. Hao, W. Si, X. X. Xi, Nature 2000, 404, 373.
- [10] A. Kinaci, C. Sevik, T. Cagin, Phys. Rev. B 2010, 82, 115114.
- [11] J. F. Schooley, W. R. Hosler, M. L. Cohen, Phys. Rev. Lett. 1964, 12, 474
- [12] M. J. Akhtar, Z.-U.-N. Akhtar, R. A. Jackson, C. R. A. Catlow, J. Am. Ceram. Soc. 1995, 78, 421.
- [13] R. A. De Souza, Adv. Funct. Mater. 2015, 25, 6326.
- [14] J. Li, S. Li, F. Liu, M. A. Alim, G. Chen, J. Mater. Sci. Mater. Electron. 2003, 14, 483.
- [15] R. A. De Souza, V. Metlenko, D. Park, T. E. Weirich, Phys. Rev. B 2012, 85, 174109.
- [16] I. Denk, F. Noll, J. Maier, J. Am. Ceram. Soc. 2005, 80, 279.
- [17] A. Ohtomo, H. Y. Hwang, Nature 2004, 427, 423.
- [18] K. Szot, W. Speier, G. Bihlmayer, R. Waser, Nat. Mater. 2006, 5, 312.
- [19] S. Shirasaki, H. Haneda, K. Arai, M. Fujimotoi, J. Mater. Sci. 1987, 22, 4439.
- [20] M. T. Buscaglia, V. Buscaglia, M Viviani, P. Nanni, M. Hanuskova, I. Eur. Ceram. Soc. 2000, 20, 1997.
- [21] R. Freer, J. Mater. Sci. 1980, 15, 803.
- [22] E. T. Park, P. Nash, J. Wolfenstine, K. C. Goretta, J. L. Routbort, J. Mater. Res. 1999, 14, 523.
- [23] P. Pasierb, S. Komornicki, M. Rekas, J. Phys. Chem. Solids 1999, 60, 1835
- [24] L. Zhang, B. Liu, H. Zhuang, P. R. C. Kent, V. R. Cooper, P. Ganesh, H. Xu, Comput. Mater. Sci. 2016, 118, 309.
- [25] J. J. Brown, Z. Ke, W. Geng, A. J. Page, J. Phys. Chem. C 2018, 122, 14590.
- [26] S. P. Waldow, A. Roger, De Souza, ACS Appl. Mater. Inter. 2016, 8, 12246.
- [27] M. Kubo, Y. Oumi, R. Miura, A. Stirling, A. Miyamoto, M. Kawasaki, M. Yoshimoto, H. Koinuma, Phys. Rev. B 1997, 56, 13535.
- [28] G. V. Lewis, C. R. A. Catlow, R. E. W. Casselton, J. Am. Ceram. Soc. 1985, 68, 555.
- [29] M. Schie, A. Marchewka, T. Müller, R. A. De Souza, R. Waser, J. Phys.: Condens. Matter 2012, 24, 485002.
- [30] J. Carrasco, F. Illas, N. Lopez, E. A. Kotomin, Yu. F. Zhukovskii, R. A. Evarestov, Yu. A. Mastrikov, S. Piskunov, J. Maier, *Phys. Rev. B* 2006, 73, 064106.



www advancedsciencenews com



- [31] J. Crawford, P. Jacobs, J. Solid State Chem. 1999, 144, 423.
- [32] C. L. Freeman, J. A. Dawson, H. Chen, J. H. Harding, L.-B. Ben, D. C. Sinclair, J. Mater. Chem. 2011, 21, 4861.
- [33] J. A. Dawson, C. L. Freeman, L.-B. Ben, J. H. Harding, D. C. Sinclair, J. Appl. Phys. 2011, 109, 084102.
- [34] J. A. Dawson, X. Li, C. L. Freeman, J. H. Harding, D. C. Sinclair, J. Mater. Chem. C 2013, 1, 1574.
- [35] Y. A. Zulueta, T. C. Lim, J. A. Dawson, J. Phys. Chem. C 2017, 121, 23642.
- [36] C. L. Freeman, J. A. Dawson, H. Chen, J. H. Harding, L.-B. Ben, D. C. Sinclair, Adv. Funct. Mater. 2013, 23, 3925.
- [37] J. A. Dawson, I. Tanaka, J. Phys. Chem. C 2014, 118, 25765.
- [38] J. A. Dawson, C. L. Freeman, J. H. Harding, D. C. Sinclair, J. Solid State Chem. 2013, 200, 310.
- [39] J. A. Dawson, H. Chen, I. Tanaka, J. Phys. Chem. C 2014, 118, 14485.
- [40] C. L. Freeman, J. A. Dawson, J. H. Harding, L.-B. Ben, D. C. Sinclair, Adv. Funct. Mater. 2013, 23, 491.
- [41] J. A. Dawson, D. C. Sinclair, J. H. Harding, C. L. Freeman, Chem. Mater. 2014, 26, 6104.
- [42] S. Piskunov, E. Kotomin, E. Heifets, J. Maier, R. Eglitis, G. Borstel, Surf. Sci. 2005, 575, 75.
- [43] G. Lewis, C. R. A. Catlow, J. Phys. C: Solid State Phys. 1985, 18, 1149.
- [44] W. Smith, T. R. Forester, J. Mol. Graph. 1996, 14, 136.
- [45] A. M. Stoneham, *Ionic Solids at High Temperatures*, World Scientific Publishing, Singapore 1989.
- [46] J. D. Gale, A. L. Rohl, Mol. Simulat. 2003, 29, 291.
- [47] T. Famprikis, P. Canepa, J. A. Dawson, M. S. Islam, C. Masquelier, Nat. Mater. 2019, https://doi.org/10.1038/s41563-019-0431-3.
- [48] J. A. Dawson, P. Canepa, T. Famprikis, C. Masquelier, M. S. Islam, J. Am. Chem. Soc. 2018, 140, 362.

- [49] J. A. Dawson, T. S. Attari, H. Chen, S. P. Emge, K. E. Johnston, M. S. Islam, Energy Environ. Sci. 2018, 11, 2993.
- [50] J. A. Dawson, H. Chen, M. S. Islam, J. Phys. Chem. C 2018, 122, 23978.
- [51] H. H. Heenen, C. Scheurer, K. Reuter, J. Voss, A. C. Luntz, J. Phys. Chem. Lett. 2019, 10, 2264.
- [52] M. S. Islam, M. Cherry, C. R. A. Catlow, J. Solid State Chem. 1996, 124, 230.
- [53] J. A. Dawson, P. Canepa, M. J. Clarke, T. Famprikis, D. Ghosh, M. S. Islam. Chem. Mater. 2019. 31, 5296.
- [54] P. A. Aparicio, J. A. Dawson, M. S. Islam, N. H. De Leeuw, J. Phys. Chem. C 2018, 122, 25829.
- [55] C. J. Xiao, Z. X. Li, X. R. Deng, Bull. Mater. Sci. 2011, 34, 963.
- [56] Y. He, Thermochim. Acta 2004, 419, 135.
- [57] D. de Ligny, P. Richet, Phys. Rev. B 1996, 53, 3013.
- [58] S. Tosawat, W. Gjindara, T. Chanchana, A. Vittaya, Chin. Phys. Lett. 2010, 27, 026501.
- [59] D. C. Sinclair, J. M. S. Skakle, F. D. Morrison, R. I. Smith, T. P. Beales, J. Mater. Chem. 1999, 9, 1327.
- [60] D. I. Woodward, I. M. Reaney, G. Y. Yang, E. C. Dickey, C. A. Randall, Appl. Phys. Lett. 2004, 84, 4650.
- [61] M.-H. Lin, J.-F. Chou, H.-Y. Lu, J. Eur. Ceram. Soc. 2000, 20, 517.
- [62] H. U. Anderson, J. Am. Ceram. Soc. 1965, 48, 118.
- [63] G. V. Lewis, C. R. A. Catlow, J. Phys. Chem. Solids 1986, 47, 89.
- [64] W. Gong, H. Yun, Y. B. Ning, J. E. Greedan, W. R. Datars, C. V. Stager, J. Solid State Chem. 1991, 90, 320.
- [65] K. Xie, N. Umezawa, N. Zhang, P. Reunchan, Y. Zhangab, J. Ye, Energy Environ. Sci. 2011, 4, 4211.
- [66] C. Yu, M. L. Scullin, M. Huijben, R. Ramesh, A. Majumdar, Appl. Phys. Lett. 2008, 92, 092118.